NUMERICAL SIMULATION OF TRANSPORT OF A HIGH-CURRENT ELECTRON BEAM GENERATED BY THE SECONDARY-EMISSION CATHODE GUN IN A DECREASING SOLENOIDAL FIELD

A.N. Dovbnya, N.A. Dovbnya, A.S. Mazmanishvili, N.G. Reshetnyak, I.A. Chertishchev
National Science Center "Kharkov Institute of Physics and Technology", Kharkov, Ukraine
E-mail: ch.igor@kipt.kharkov.ua

The software tool has been developed for computing the electron beam formation by means of the secondary-emission cathode magnetron gun in the electron energy range between 30 and 65 keV at beam transport in a decreasing magnetic field of the solenoid. Numerical simulation data on the tubular electron flow motion and visualization are presented. The beam current was investigated versus the amplitude and gradient of the field decrease, and also, versus the initial beam particle distribution in the phase space. It has been found that for the given simulation conditions, the magnetic field reconfiguration has an effect only on the total displacement of the electron beam, without causing a noticeable change in the shape of the final flow distribution along the longitudinal coordinate.

PACS: 29.27.Fh

INTRODUCTION

At present, there is a strong trend in many countries towards developing and introducing commercially the beam methods of materials processing by energy fluxes. In this direction, modification of metal/alloy surface characteristics, radiation-chemical modification of polymer materials can be identified as tasks of high importance [1, 2]. For example, when treated with an electron beam, some types of steel used in automobile industry have shown a 2- to 5-fold increase in microhardness, and accordingly, in service life. The electron beam treatment of electric-generator gas turbine blades increased their operation life by more than two times [3]. To accomplish the mentioned tasks, a wide use is made of the accelerators generating intense electron beams of energies 100 to 400 keV [4].

The NSC KIPT team has created the electron accelerator [5] based on the magnetron gun with a metal cold secondary-emission cathode. The operation of these guns relies on secondary-emission multiplication of electrons, electron cloud formation and electron beam generation in crossed electric and magnetic fields.

The present paper reports the results from studies into the influence of the initial state of the electron beam generated by the secondary-emission cathode magnetron gun (SECMG) on the final beam distribution. Theoretical and experimental data are presented on the radial electron beam formation by the SECMG during the beam transport in the decreasing magnetic field of the solenoid, and also, the mathematical model of the electron beam motion in this field is constructed. The feasibility of inner cylindrical surface irradiation has been investigated. When considering particle flows with the oversized phase volume of the initial quantities, in particular, with large vertical and radial dimensions Δz_0, Δr_0, and at a wide pulse straggling, p_{z0} and p_{r0}, it was demonstrated that one may expect a corresponding increase in the vertical ring area Δz_U, within which the condition of beam falling on the prescribed radius is fulfilled. Note that the physical object under consideration differs in that it provides the possibility to compare the data obtained during the observations with the data found in the process of mathematical modeling.

EXPERIMENTAL SETUP

The paper is concerned with the formation of a radial electron beam by the SECMG, and the measurements of beam parameters during its transport in the decreasing magnetic field of the solenoid. The experiments were performed at the setup described in [5].

For energizing the magnetron gun, a pulse generator was used, which provided voltage pulses with a spike of ~100 kV, pulse flat-part amplitude ~70 kV, pulse length ~20 μs. The electron source is located in the vacuum volume. For electron beam production, a magnetron gun, with the Ø78 mm anode and the Ø36 mm cathode, was used. The magnetic field for the electron beam generation and transport is created by the solenoid consisting of 4 coils, which are energized by dc sources. By varying the current in each of the coils, it was possible to change the amplitude and longitudinal distribution of the magnetic field along the axis of the magnetron gun and the beam transport channel. This provided different modes of electron beam formation.

The beam transport was realized in the system consisting of 14 copper rings with an inner diameter of ~66 mm, located at ~85 mm from the magnetron gun edge. The rings, 8 mm in width, were spaced at intervals of 1.5 mm. The system is located in the magnetic field created by the solenoid. Besides, to provide a local change in the rate of the solenoidal field decrease, a scattered magnetic field created by $SmCo_5$ annular magnets was used. The magnets were placed along the axis of the system, behind the 14th ring.

Fig. 1 shows the beam transport channel used in the studies.

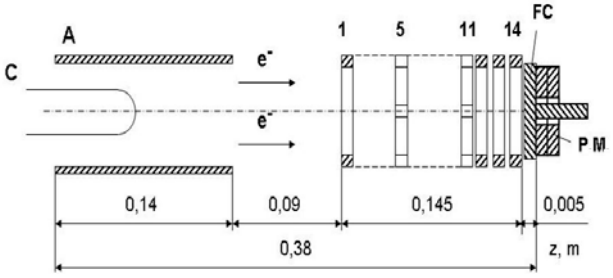

Fig. 1. Beam transport diagram: A – anode; C – cathode; FC – Faraday cup; PM – permanent magnets

Fig. 2 illustrates three magnetic field amplitude distributions: H_0, H_+ and H_-. Here H_0 is the magnetic field of the main solenoid, H_+ is the combined field of both the solenoid and the magnet (field directions are the same), H_- is the combined field of the main solenoid and the additional magnet (the fields are oppositely directed). In this case we have $H_+ + H_- = 2H_0$.

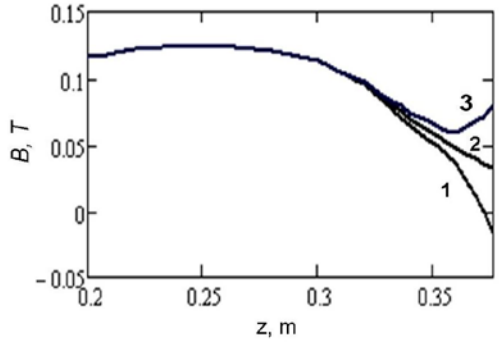

Fig. 2. Magnetic field distribution along the beam transport channel: 1 – combined field H_-; 2 – main solenoid field H_0; 3 – combined field H_+

The major field differences take place at the periphery of the vertical transport channel.

DATA PREPARATION FOR MODELING

In the process of computational modeling, it is necessary to prepare the arrays of the quantities, which are in essence statistically distributed. Among these quantities, we mention above all the particle energy E and the initial radius of the particles, r_0.

The sample of random particle energy values, $\{E_n\}$, is determined as a set of numerical solutions to the equation

$$\int_0^{E_n} f_E(\varepsilon)\, d\varepsilon = u_n, \quad n = 1,..., N, \qquad (1)$$

where E_n is the successive particle energy value, $f_E(\varepsilon)$ is the density of particle energy distribution, u_n is the successive realization of the standard generator of random values uniformly distributed within the interval (0; 1).

Fig. 3 shows the experimental data N_ε and the result $P(\varepsilon)$ of their interpolation used as an analog of the density $f_E(\varepsilon)$.

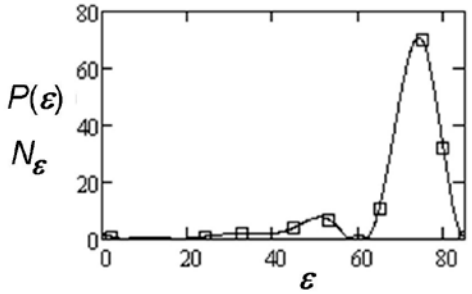

Fig. 3. Electron energy distribution: experimental data N_ε (small squares) and the spline interpolation data $P(\varepsilon)$ (line)

Fig. 4 shows the obtained sample of N = 1000 particles in volume.

Fig. 5 shows the corresponding histogram $G(\varepsilon)$ of the generated random values employed further in modeling.

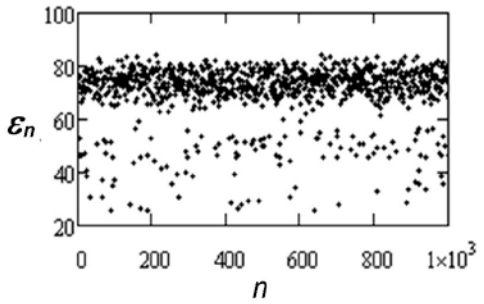

Fig. 4. Electron energy distribution: sample of N

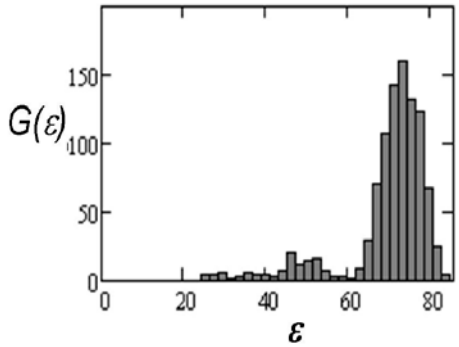

Fig. 5. Electron energy distribution: histogram $G(\varepsilon)$ of the generated random values

On emission, the particles escape from the ring having the inner radius r_a and the outer radius r_b. Assuming the emitted particle density on the ring surface to be constant, and using the Cartesian variables x and y, we write down the density $f_{XY}(x, y)$ in terms of the Cartesian coordinates as

$$f_{XY}(x, y) = \left[2\pi(r_b^2 - r_a^2)\right]^{-1}. \qquad (2)$$

In polar coordinates, after azimuth integration, this density is written in the form:

$$f(r_0) = 2r_0\left(r_b^2 - r_a^2\right)^{-1}. \qquad (3)$$

Fig. 6 shows the distribution density $f(r_0)$ at r_a = 0.018 *m* and r_b =0.022 *m*.

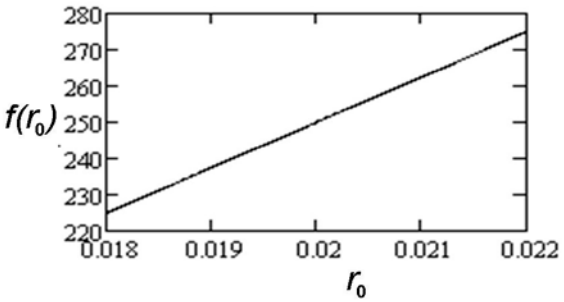

Fig. 6. Initial radial distribution of particles: radial distribution density $f(r_0)$

Therefore, the sample of random values of initial particle radius, $\{r_0\}$, is determined as a set of numerical solutions of the equation

$$\int_{r_a}^{r_{0,n}} f(r_0)\, dr_0 = w_n, \quad n = 1,..., N, \qquad (4)$$

to give

$$r_{0,n} = \left[r_a^2 + w_n\left(r_b^2 - r_a^2\right)\right]^{1/2}, \; n = 1,..., N, \qquad (5)$$

where $r_{0,n}$ is the succeeding initial radius value of the particle, w_n is the succeeding realization of the genera-

tor of random values uniformly distributed within the interval (0; 1).

Fig. 7 shows the obtained sample of volume N=1000 particles.

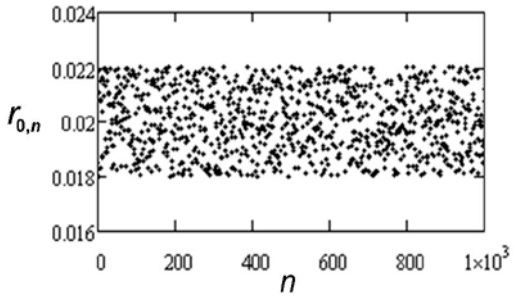

Fig. 7. Initial radial r_0 distribution of particles: N=1000 sample

Fig. 8 shows the corresponding histogram $G(r_0)$ of the random values further used in modeling.

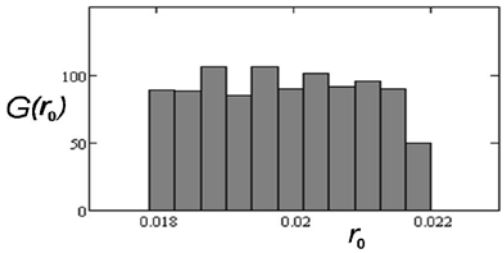

Fig. 8. Initial radial distribution $G(r_0)$ of particles: generated sample histogram

THE MATHEMATICAL MODEL

The mathematical model of the problem under discussion can be considered in terms of the Hamiltonian, which has the following form in the cylindrical coordinate system (r, z, ϑ):

$$H = \frac{p_r^2 + p_z^2}{2m} + \frac{1}{2m}\left(\frac{p_\vartheta}{r} - e_0 A(r,z)\right)^2, \qquad (6)$$

where e_0, m are, respectively, the charge and rest mass of the electron; p_r, p_z, p_ϑ are the canonical momenta; A is the magnetic potential.

Taking account of the azimuthally symmetry, the latter can be written for now as $A(r,z) = Brf(z)$, where $f(z)$ is the longitudinal coordinate function, which will be dealt with below; B is the magnetic field strength at the selected point. The magnetic field function $A(r,z)$ can be defined relying on both the theoretical assumptions and empirical observations. In numerical calculations, in the process of algorithm single-stepping, each time it is necessary to preset the function $A(r,z)$ value on the current coordinate z, and also, to determine the value of its derivative $\partial A(r,z)/\partial z$.

In the general case, the statement of initial conditions along with the Hamiltonian, which includes the magnetic potential $A(r,z)$, appears to be sufficient for solving the direct problem of single-particle trajectory tracing, and so, for solving the direct problem of electron beam dynamics. On the other hand, by purposefully adjusting the magnetic field distribution (see Fig. 2) and the set of initial conditions, it turns out possible to control the parameters of the resultant beam.

For the canonical momenta p_r, p_z, we write down: $p_r = m\dot{r}$, $p_z = m\dot{z}$, $p_\vartheta = mr^2\dot{\vartheta}$, where the point over the variables denotes differentiation with respect to the current time. Let us use the Hamiltonian form of the motion equations for the coordinates and electron moment a that have the general form. This gives

$$\begin{cases} \dot{r} = p_r/m, \\ \dot{z} = p_z/m, \\ \dot{\vartheta} = \dfrac{1}{mr}\left(\dfrac{p_\vartheta}{r} - e_0 Brf(z)\right), \\ \dot{p}_r = \dfrac{1}{m}\left(\dfrac{p_\vartheta}{r} - e_0 Brf(z)\right)\left(\dfrac{p_\vartheta}{r^2} + e_0 Bf(z)\right), \\ \dot{p}_z = \dfrac{1}{m}\left(\dfrac{p_\vartheta}{r} - e_0 Brf(z)\right)\left(e_0 Br\dfrac{\partial}{\partial z} f(z)\right), \\ \dot{p}_\vartheta = 0. \end{cases} \qquad (7)$$

As a result, in set (7) we have the equations for both the coordinates and the canonical momenta. In this set, we choose as constant amplitude of B a certain magnetic field value on the solenoid axis. Note that in the set of equations (7) there are the variables, the values of which differ by many orders of magnitude. To put these decimal exponents in equilibrium, we turn, making use of the light speed c, from the current time t to the variable $s = ct$. This variable may be interpreted as the path travelled by the particle, and the derivative with respect to s will be denoted by a prime mark. Besides, the canonical momenta p_r, p_z, p_ϑ are replaced by $p_r = e_0 Bq_r$, $p_z = e_0 Bq_z$, $p_\vartheta = e_0 Bq_\vartheta$.

Equations (7) must be complemented with the initial conditions for r_0, z_0, ϑ_0, and also for q_{r0}, q_{z0}, $q_{\vartheta 0}$. In each of the lines of set (7), one can separate the Larmor factor $\mu = e_0 B/mc$, and also, the function $f(z)$ of the longitudinal coordinate, and accordingly, the function $Bf(z)$ that describes the magnetic field strength along the z-axis. It is convenient that the amplitude B should be chosen one time only in such a way that the function $Bf(z)$ might be used within the whole interval of possible z values. Based on the experimental data (Fig. 2), and using the three-point approximation, we have constructed the functions $f(z)$ and $\partial f(z)/\partial z$, which describe the magnetic field on the solenoid axis.

When elaborating the computational algorithm, it is essential to provide, on the one hand, its unconditional convergence, and, on the other hand, the rapidity of its time realization. That will permit modeling for a rather large number of particles, N (about 1000).

The numerical solution algorithm stability is connected with the space integration step Δs and the Larmor parameter μ. Under the condition $\mu\Delta s << 1$, the convergence of computational solution of set (7) to its analytical analog can be expected. Since e_0/mc =586.69, then at $B = 0.2$ T we obtain $e_0 B/mc$ =117.34 m^{-1}. Then the condition $\mu\Delta s << 1$ will be fulfilled provided that $\Delta s << 0.0001$ m.

Now, from the computational viewpoint, the problem for one particle can be defined as the Cauchy problem, i.e., the problem of finding the solution for the set of ordinary differential equations with prescribed initial conditions. As a result, we obtain the electron trajectory, which meets six initial requirements.

On requiring the fulfillment of the prescribed condition (e.g., reaching a certain R_U value by the radial component *r*), it appears possible, by holding fixed the values of other components of the electron trajectory, to form the resulting beam and investigate its properties.

EXPERIMENTAL AND SIMULATED RESULTS

Fig. 9 shows the magnetic field distributions in the peripheral region and the respective trajectories of particles. In their representative capacity, we have chosen 10 particles, which at the start were uniformly distributed in azimuth ϑ. It can be seen that the electron beam as a whole experiences rotation in the azimuth ϑ.

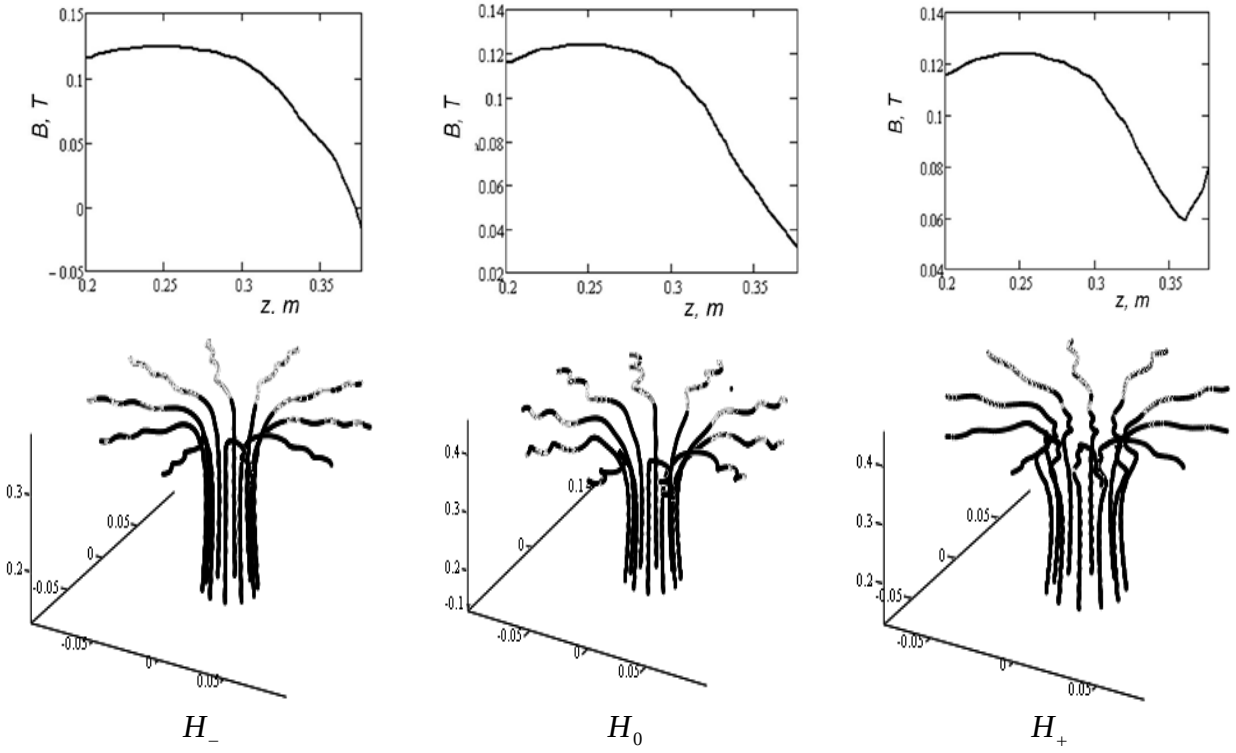

Fig. 9. Magnetic field distribution B in the peripheral region of the beam transport channel for different field directions of the permanent magnet H_-, H_0 and H_+ (curves above), and the respective particle trajectories (bottom figures, where the z-axis is vertical)

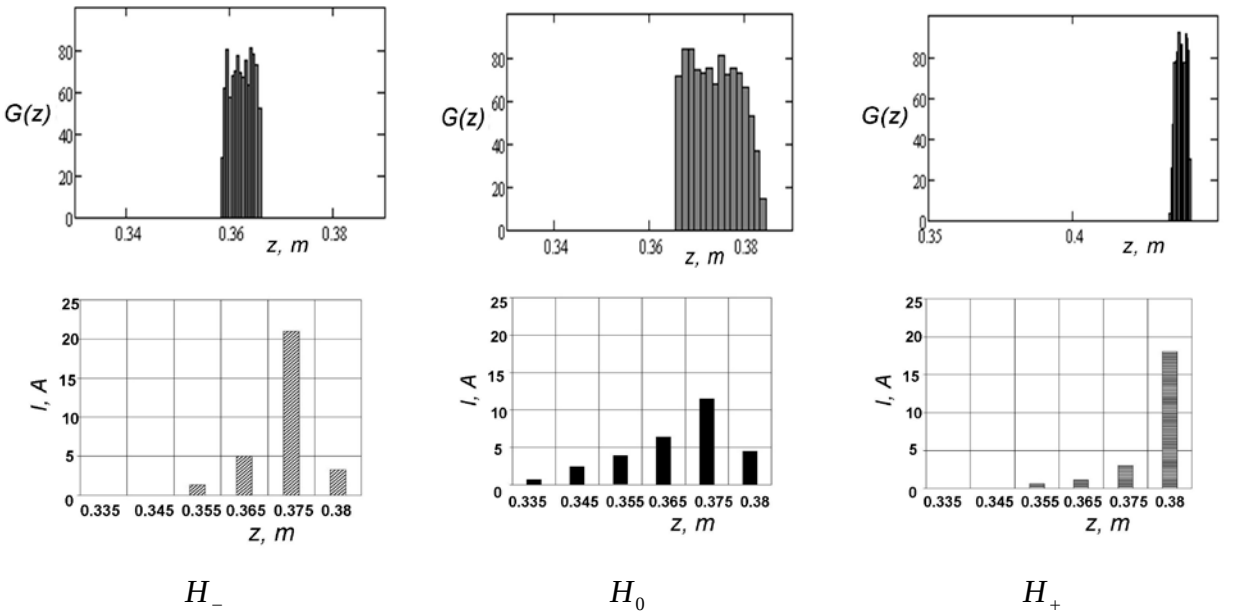

Fig. 10. Computed histograms $G(z)$ of vertical z values of electrons after they reach the threshold radius R_U (upper figures); current distributions on the measuring lamellae and the Faraday cup (lower figures); the corresponding fields H_-, H_0 and H_+ are indicated

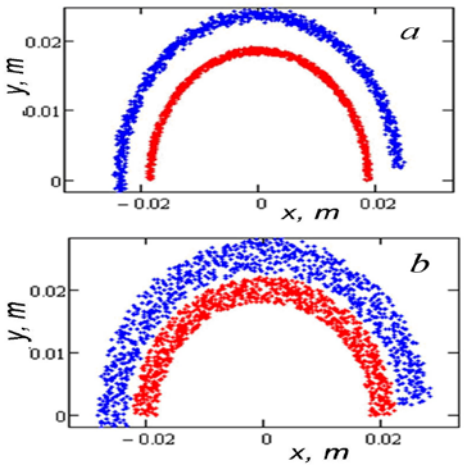

Fig. 11. Particle trajectory cross-sections for two different radii of the semi-ring; a – r_b =19 mm; b – r_b =22 mm (red points are starting, blue points are finishing)

We now fix the moment, when the radial component reaches the value R_U=33 mm. As each electron reaches this level, we form the file of longitudinal coordinates Z_U at the moment and using it as a basis, construct the histogram of the distribution *G(Z)*.

Fig. 10 shows the computed histograms *G(Z)* of vertical Z values of the electrons after they reach the threshold radius R_U (upper figures). The histograms were computed for three magnetic field cases corresponding to the curves shown in Fig. 2. The field sequence order in the figures (H_{--}, H_0, H_+) has been chosen so that the field amplitudes in the peripheral region should increase. The corresponding current distributions on the measuring lamellae are indicated in each of the lower figures. From Fig. 10 it can be seen that at the chosen H_- field variant, 70% of current falls on the 14th ring of width 8 mm, which is in the vicinity of the maximum gradient of the field decrease. It is also evident that at the chosen H_+ field variant, the beam particles, which pass along the axis of the channel, mainly fall axially on the collector.

This figure suggests the conclusion that each of the particles in its motion to the peripheral region is displaced radially. This tendency can be seen in Fig. 11 showing trajectories for particles, which are uniformly distributed at the start within the interval (0, π). The particles are emitted from the cathode ring having the inner radius r_a =18 mm and the outer radius r_b (two variants for comparison).

We now introduce the field parameter η in such a way that the next current amplitude of the magnetic field is equal to $H(\eta) = H_0 + \eta(H_+ - H_0)$.

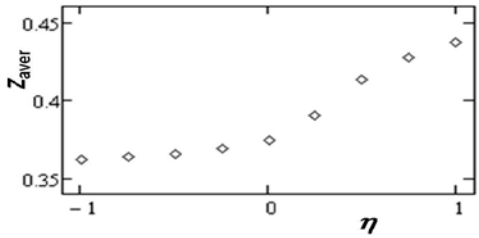

Fig. 12. Mid-beam on the target versus magnetic field distribution

Fig. 12 shows the computed coordinates of the beam center of mass Z_{aver} on the inner cylindrical surface versus the parameter η, i.e., versus the magnetic field variation in the peripheral region.

CONCLUSIONS

We have presented the results of experimental studies and simulation data on the radial electron beam formation and steering by the magnetron gun with a secondary-emission cathode in the electron energy range from 30 to 65 keV; and also, the measured data on the parameters of the beam during its transport in the total decreasing magnetic field of the solenoid and the field of the steering permanent magnet. Results of computational modeling for the motion of a tubular electron flow have been given. It has been shown that the current value and its distribution along the length of the rings are dependent on the amplitude of the magnetic field distribution along the axis of the system and the gradient of the magnetic field decrease. It has been found that at the given initial conditions for the beam particles and the longitudinal magnetic field distributions along the gun axis and the transport channel, the beam flow comes to the vertical ring area, about 1 cm in length. The given simulated results are in agreement with the experimental data for the H_{--}, H_0 and H_+ field cases. Thus, the experiments and computational modeling have demonstrated the possibility of beam positioning on the vertical wall by varying the magnetic field amplitude.

REFERENCES

1. M.F. Vorogushin, V.A. Glukhih, G.S. Manukyan, et al. Beam and ion-plasma technology // *Problems of Atomic Science and Technology. Series "Physics of Radiation Effects and Radiation Materials Science"*. 2012, № 3, p. 101-109.
2. A.N. Dovbnya, S.D. Lavrinenko, V.V. Zakutin, et al. Surface modification of zirconium alloy Zr1%Nb electron beam accelerator based on magnetron gun // *Problems of Atomic Science and Technology. Series "Physics of Radiation Effects and Radiation Materials Science"*. 2011, № 2, p. 39-45.
3. V.A. Glukhih, O.P. Pecherskyi, V.I. Engelko, et al. Modification of surface properties of materials with powerful pulsed electron beams // *Proceedings of the 10th International Conference on Applied Charged Particle Accelerators in Medicine and Industry* (*St.-Petersburg, Russia*). 2001, p. 445-447.
4. V. Engelko, G. Mueller, A. Andreev, et al. Pulsed Electron Beam Facilities (GESA) for Surface Treatment // *Proceedings of the 10th International Conference on Applied Charged Particle Accelerators in Medicine and Industry* (*St.-Petersburg, Russia*). 2001, p. 412-417.
5. A.N. Dovbnya, V.V. Zakutin, N.G. Reshetnyak, et al. Investigation of beam production in accelerator with secondary-emission source for material surface treatment // *Journal of Kharkiv National University. Physical series "Nuclei, Particles, Fields"*. 2006, № 732, Iss. 2(30), p. 96-100.

Article received 06.10.2015

ЧИСЛЕННОЕ МОДЕЛИРОВАНИЕ ТРАНСПОРТИРОВКИ СИЛЬНОТОЧНОГО ЭЛЕКТРОННОГО ПУЧКА, ФОРМИРУЕМОГО МАГНЕТРОННОЙ ПУШКОЙ С ВТОРИЧНО-ЭМИССИОННЫМ КАТОДОМ, В СПАДАЮЩЕМ МАГНИТНОМ ПОЛЕ СОЛЕНОИДА

А.Н. Довбня, Н.А. Довбня, А.С. Мазманишвили, Н.Г. Решетняк, И.А. Чертищев

Разработано программное средство для расчета формирования электронного пучка магнетронной пушкой с вторично-эмиссионным катодом в диапазоне энергий электронов 30…65 кэВ при транспортировке в спадающем магнитном поле соленоида. Приведены результаты численного моделирования по движению и визуализации трубчатого электронного потока. Изучена зависимость тока пучка от амплитуды и градиента спада поля, а также начального распределения частиц пучка в фазовом пространстве. Показано, что для рассмотренных условий моделирования изменение конфигурации магнитного поля влияет только на общее смещение пучка электронов, но не приводит к заметному изменению вида итогового распределения потока по продольной координате.

ЧИСЕЛЬНЕ МОДЕЛЮВАННЯ ТРАНСПОРТУВАННЯ ПОТУЖНОСТРУМОВОГО ЕЛЕКТРОННОГО ПУЧКА, ЩО ФОРМУЄТЬСЯ МАГНЕТРОННОЮ ГАРМАТОЮ З ВТОРИННО-ЕМІСІЙНИМ КАТОДОМ, У СПАДАЮЧОМУ МАГНІТНОМУ ПОЛІ СОЛЕНОЇДА

А.М. Довбня, Н.А. Довбня, О.С. Мазманішвілі, М.Г. Решетняк, І.О. Чертіщев

Розроблено програмний засіб для розрахунку формування електронного пучка магнетронною гарматою з вторинно-емісійним катодом у діапазоні енергій електронів 30...65 кеВ при транспортуванні в спадаючому магнітному полі соленоїда. Наведено результати чисельного моделювання руху і візуалізації трубчастого електронного потоку. Вивчено залежність струму пучка від амплітуди і градієнта спаду поля, а також початкового розподілу частинок пучка в фазовому просторі. Показано, що для розглянутих умов моделювання зміна конфігурації магнітного поля впливає тільки на загальний зсув пучка електронів, однак не призводить до помітної зміни виду підсумкового розподілу потоку по повздовжній координаті.